

Instability of the miscible magnetic/non-magnetic fluid interface

Mikhail S. Krakov^{1,†}, Arthur R. Zakinyan² and Anastasia A. Zakinyan²

¹Belarusian National Technical University, 4 Nezavisimosti Ave., Minsk 220013, Belarus

²North-Caucasus Federal University, 1 Pushkin Street, Stavropol 355017, Russia

(Received 25 August 2020; revised 12 December 2020; accepted 13 December 2020)

The behaviour of the diffusion front of a magnetic fluid in contact with a miscible non-magnetic fluid in a normal magnetic field is studied. It was found that the magnetic field is a cause of the diffusion front bending and its movement accompanied by intense advective flows. These flows lead to the fast growth of the wavy shape of the diffusion front and formation of the peaks. This phenomenon is studied both numerically and experimentally. The reasons for the instability of the diffusion front in a magnetic field are discussed. The influence of the parameters of the problem (Schmidt number, magnetic Rayleigh number, magnetic field, the thickness of the layer, diffusion front width, etc.) on the instability parameters is studied both numerically and experimentally. It is shown that the studied instability differs from Rosensweig's instability.

Key words: contact lines, fingering instability, magnetic fluids

1. Introduction

The interface between two miscible fluids is a very interesting object of study, since various processes are concentrated there. Diffusion and advective flows are initiated at the interface by differences in the concentration of the two fluids; therefore, various instabilities due to different mechanisms (double diffusion, chemical reactions, thermodiffusion) have been found (Hurle & Jakeman 1971; Schechter, Prigogine & Hamm 1972; Turner 1985; Bratsun *et al.* 2015). One additional tool can be used to initiate instability of the diffusion front when fluids have magnetic properties: this is a magnetic field. The magnetic fluid is a colloidal solution in a carrier fluid of ferromagnetic particles approximately 10 nm in size (Berkovsky, Medvedev & Krakov 1993). To prevent aggregation under the action of magnetic forces, the particles are coated with a surfactant layer. Such fluids are very stable and used for numerous applications, such as seals, loudspeakers, shock absorbers and lubricants (Berkovsky *et al.* 1993). One of the

† Email address for correspondence: mskrakov@gmail.com

promising applications of magnetic fluids is the controlled delivery of medicines to the affected organ. Magnetic fluid is used as a carrier fluid controlled by a magnetic field and drugs are mixed with a magnetic fluid before the fluid is injected. In this case, there is a problem of mixing the miscible magnetic fluid and the drug, since the velocities of the fluids in the injection tube are very small, flow is stable and hydrodynamic mixing mechanisms are not effective.

The instability of the interface between miscible magnetic and non-magnetic fluids has been studied for different cases in a number of papers. Magnetic field driven micro-convection in the Hele-Shaw cell was studied in Cebers & Igonin (2002), Erglis *et al.* (2013) and Kitenbergs *et al.* (2015). Mixing for microfluidics was studied simultaneously (Kitenbergs *et al.* 2018). In these studies, the magnetic field was oriented perpendicular to the plane of the Hele-Shaw cell and parallel to the fluid interface. Mixing occurred in a microchannel in which fluids flowed. The instability of the diffusion front in a magnetic field perpendicular to the interface for the case of infinite layers was studied in the frame of linear theory (Erglis *et al.* 2013). In this study, it was found that the plane step-like diffusion front under the action of a magnetic field is unstable. For a linear dependence of magnetization on the magnetic field, the critical value of the magnetic Rayleigh number and the critical wave number were found. However, the effect of the nonlinear character of the fluid properties and the magnitude of the magnetic field on the instability parameters remain unknown. Moreover, it is unknown whether the final structures are stable or whether the concentration convection continues to mix fluids. The intensity of mixing is also unknown. Only an experiment (both numerical and physical) can give answers to these questions.

In recent years, various methods have been studied widely for micromixing of the fluids in microfluidic devices and lab-on-a-chip (Cai *et al.* 2017). The magnetic field is also used as an active micromixer. The mixing of two miscible fluids (magnetic and diamagnetic) in the flow was investigated experimentally and numerically (Zhu & Nguyen 2012) with the field oriented normally to the interface. In this paper, it was found that a magnetic field rapidly mixes magnetic and non-magnetic fluids by magnetically induced secondary flow in the chamber. Numerical analysis of magnetic nanoparticle transport in microfluidic systems under the influence of a non-uniform magnetic field is presented in Cao, Han & Li (2012). This study demonstrated that a non-uniform magnetic field can increase the concentration of particles in a given place, but does not contribute much to mixing. Therefore, the same authors later (Cao, Han & Li 2015) studied the mixing of miscible fluids in the flow, adding an alternative uniform magnetic field to the non-uniform field of conductors. It was shown that mixing in this situation is very intense. However, it remained unclear whether an alternating magnetic field is capable of mixing miscible fluids only in combination with a non-uniform field or if the role of a non-uniform field is not very important.

The aim of the present study is to reveal the main factors affecting the instability of the interface of miscible magnetic and non-magnetic fluids. A better understanding will reveal the circumstances under which magnetic mixing might be effectively used in meso- and microfluidic systems.

2. Formulation of the problem and governing equations

Characteristic sizes of meso- and microfluidic systems are less than one millimetre and hundreds of microns, respectively. The kinematic viscosity of fluids in these systems is more than $10^{-6} \text{ m}^2 \text{ s}^{-1}$. The flow velocity is approximately 1 mm s^{-1} . This means

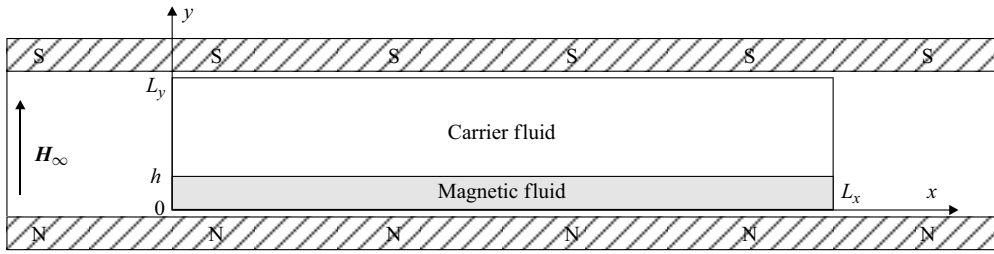


Figure 1. Geometry of the problem.

that the Reynolds number Re is less than one, the flow is creeping and hydrodynamic instabilities, such as the Kelvin–Helmholtz instability, do not occur. In this case, the main mechanism responsible for the mixing of fluids is diffusion and the influence of the flow can be neglected.

Thus, in this paper, as a model, we consider a two-dimensional closed rectangular container with a height L_y and ratios of length to height of 10 : 1 and 15 : 1 (figure 1). The container is filled with a magnetic fluid at a height of h , for example, a quarter of the height of the container, and the rest of the volume of the container is filled with a pure carrier fluid. The ratio of the length of the magnetic fluid layer to its height is rather high in order that the edge effects will hopefully not be dominant regarding the advective flows. The container is in the field of gravity. The density of the magnetic fluid ρ_{mf} is

$$\rho_{mf} = \rho_p c + \rho_f(1 - c), \tag{2.1}$$

where c is the volume concentration of the particles together with the surfactant layer, ρ_p is the density of these particles, ρ_f is the density of the carrier fluid, $\rho_p > \rho_f$. Since $\rho_{mf} > \rho_f$, the magnetic fluid occupies the lower part of the container. The container is in an external constant magnetic field, uniform at ‘infinity’ (boundaries of the calculation domain) and oriented vertically.

The magnetic field is described by the Maxwell equations:

$$\nabla \cdot \mathbf{B} = 0, \quad \nabla \times \mathbf{H} = 0, \quad \mathbf{B} = \mu_0(\mathbf{H} + \mathbf{M}(H)). \tag{2.2a-c}$$

The equation of state $M(H)$ for a magnetic fluid is given in the form which is the best approximation for the magnetization of real magnetic fluids (Vislovich 1990):

$$\mathbf{M} = M(H) \frac{\mathbf{H}}{H}, \quad M(H) = M_S \frac{\chi_0 \hat{H}}{1 + \chi_0 \hat{H}} \frac{c(x, y, t)}{c_0} = M_{Sf}(\hat{H}) \frac{c(x, y, t)}{c_0}, \tag{2.3a,b}$$

where the dimensionless strength of the magnetic field is $\hat{H} = H/M_S$, M_S is the saturation magnetization of a magnetic fluid, c is the volume concentration of magnetic particles at a given point at a given time in the solution, c_0 is the initial concentration of magnetic particles in the magnetic fluid and χ_0 is the initial magnetic susceptibility of the magnetic fluid.

According to the equation $\nabla \times \mathbf{H} = 0$ we can use a magnetic potential F ($\mathbf{H} = \nabla F$). Taking into account (2.3a,b), the equation for the magnetic potential due to $\nabla \cdot \mathbf{B} = 0$ and

the equation of state can be expressed as

$$\left. \begin{aligned} \nabla(\mu \nabla F) &= 0, \\ \mu &= \left(1 + \frac{\chi_0}{1 + \chi_0 \hat{H}}\right) \frac{c(x, y, t)}{c_0}, \end{aligned} \right\} \quad (2.4)$$

where μ is the relative magnetic permeability.

The boundary conditions for the magnetic potential at the borders of the container are

$$(\mu \nabla F_i - \nabla F_e) \cdot \mathbf{n} = 0, \quad (\nabla F_i - \nabla F_e) \times \boldsymbol{\tau} = 0, \quad (2.5a,b)$$

where \mathbf{n} and $\boldsymbol{\tau}$ are the vectors normal and tangential to the walls of the container, and the indices 'i' and 'e' refer to the area inside and outside the container, respectively.

As the outer vertical magnetic field H_∞ is uniform and oriented along the axis y, the magnetic potential at all outer borders of the computation domain can be written as

$$F = H_\infty y. \quad (2.6)$$

As the density of the mixture is described by the expression (2.1), then, by analogy with the coefficient of thermal expansion $\beta = -(1/\rho)\partial\rho/\partial T$, we use the solutal expansion coefficient $\beta_c = (1/\rho)\partial\rho/\partial c$ (Eckert, Acker & Shi 2004; Islam, Sharif & Carlson 2013). In this case

$$\beta_c = \frac{\rho_p - \rho_f}{\rho_f + (\rho_p - \rho_f)c} = \frac{1}{c + \rho_f/(\rho_p - \rho_f)}. \quad (2.7)$$

As $c \rightarrow 0$, $\beta_c \rightarrow \beta_c^0 = (\rho_p - \rho_f)/\rho_f$, and then expression (2.7) can be rewritten in the form

$$\beta_c = \beta_c^0 \frac{1}{1 + \beta_c^0 c}. \quad (2.8)$$

Note that, unlike the coefficient of thermal expansion, the coefficient β_c^0 is not small. For magnetic fluids with magnetite particles with a diameter of $d_m = 10$ nm as a dispersed phase, covered with a layer of oleic acid with a thickness of $d_h = 2$ nm, the average particle density can be estimated as

$$\begin{aligned} \rho_p &= \frac{\rho_m d_m^3 + \rho_h [(d_m + 2d_h)^3 - d_m^3]}{(d_m + 2d_h)^3} \\ &\approx \frac{5.5 \times 10^3 + 0.9 \times (14^3 - 10^3)}{14^3} = 2.6 \times 10^3 \text{ kg m}^{-3}. \end{aligned} \quad (2.9)$$

Then, for hydrocarbon liquids and mineral oils, for which the density is $\rho_f = 0.8\text{--}1.0 \times 10^3 \text{ kg m}^{-3}$, the coefficient β_c^0 takes values from 1.6 to 2.2.

The equation of motion of the incompressible magnetic fluid has the form (Berkovsky *et al.* 1993)

$$\rho_{mf} \left(\frac{\partial u_i}{\partial t} + u_k \frac{\partial u_i}{\partial x_k} \right) = -\frac{\partial p}{\partial x_i} + \frac{\partial}{\partial x_k} \left[\eta \left(\frac{\partial u_i}{\partial x_k} + \frac{\partial u_k}{\partial x_i} \right) \right] + \rho_{mf} g_i + \mu_0 M \frac{\partial H}{\partial x_i}, \quad (2.10)$$

or, in vector form (where $\eta(c)$ is the dynamic viscosity)

$$\rho_{mf} \left[\frac{\partial \mathbf{u}}{\partial t} + (\mathbf{u} \cdot \nabla) \mathbf{u} \right] = -\nabla p + \eta \Delta \mathbf{u} + 2(\nabla \eta \cdot \nabla) \mathbf{u} + \nabla \eta \times (\nabla \times \mathbf{u}) + \rho_{mf} \mathbf{g} + \mu_0 M \nabla H. \quad (2.11)$$

The term $2(\nabla \eta \cdot \nabla) \mathbf{u}$ is important when the viscosity of a fluid is not constant. The first viscous term is of the order of $\eta u/\lambda^2$, where λ is the some characteristic length,

for example, the wavelength of perturbations of the diffusion front. The second term is of the order of $(\Delta\eta/\delta)(u/\lambda) = (\Delta\eta u)/\delta\lambda$, where $\Delta\eta$ is the change in viscosity over the characteristic length δ , for example, the width of the diffusion front. In almost the entire calculation domain under consideration, with the exception of the diffusion front, the viscosity is constant and the second term $2(\nabla\eta \cdot \nabla)\mathbf{u}$ can be neglected. In the diffusion front, this term is insignificant if $\Delta\eta/\eta \ll \delta/2\lambda$. In our study, as will be seen below, $\delta/2\lambda \sim 0.03\text{--}1$. Since $\Delta\eta$ is at least of the order of $2.5c\eta_0$ (from Einstein's formula), this condition is satisfied only for low concentrations $c \ll \delta/5\lambda$. However, from the point of view of the influence on the flow structure, the volume of the liquid in the diffusion front is very small and, from our point of view, the term $2(\nabla\eta \cdot \nabla)\mathbf{u}$ can be neglected in the entire volume of the liquid, including the diffusion front. Moreover, this assumption becomes reasonable if we take into account that the velocity vector is directed normally to the line of the diffusion front (as will be seen from figure 8), and due to the continuity equation $\partial u/\partial n \rightarrow 0$ at the diffusion front (n is the normal direction). As the term $2(\nabla\eta \cdot \nabla)\mathbf{u}$ in the diffusion front can be written as $(\partial\eta/\partial n)(\partial u/\partial n)$, it also tends to zero. Since the viscosity in the magnetic fluid and the upper fluid can differ significantly, we leave the concentration dependence in the dynamic viscosity coefficient before the velocity Laplacian.

The third term can be written as $\nabla\eta \times \boldsymbol{\omega}$. As vector $\nabla\eta$ is oriented normally to the line of the diffusion front and the vorticity vector $\boldsymbol{\omega}$ is oriented normally to the plane of $n\tau$ (coordinate τ oriented along the diffusion front, and n normally), then their vector product is oriented along the diffusion front. In this case, the action of this term cannot influence the movement of the diffusion front in the normal direction. So, this term can be neglected. Another argument for neglecting this term follows. When we pass from natural variables to the new variables, the streamfunction and vorticity, we apply the $(\nabla \times)$ -operator to the equation of motion. In this case, the value of the term $\nabla\eta \times \boldsymbol{\omega}$ is $(\partial\eta/\partial\tau)(\partial\omega/\partial\tau) - (\partial\eta/\partial n)(\partial\omega/\partial n)$ (since $\nabla \times \nabla\eta = 0$). Along the diffusion front viscosity does not change, $\partial\eta/\partial\tau \rightarrow 0$. As the velocity is oriented normally to the diffusion front and almost does not change in the area of the front, $\partial\omega/\partial n \rightarrow 0$. Thus, the third term tends to zero too.

Thus, we use the equation of motion in the form

$$\rho_{mf} \left[\frac{\partial \mathbf{u}}{\partial t} + (\mathbf{u} \cdot \nabla)\mathbf{u} \right] = -\nabla p + \eta(c)\Delta\mathbf{u} + \rho_{mf}\mathbf{g} + \mu_0 M \nabla H. \quad (2.12)$$

The density of the magnetic fluid, taking into account the definition of the value β_c^0 , can be rewritten based on (2.7)

$$\rho_{mf}\beta_c = \rho_p - \rho_f = \beta_c^0 \rho_f. \quad (2.13)$$

Taking into account expression (2.8), we obtain

$$\rho_{mf} = \rho_f(1 + \beta_c^0 c). \quad (2.14)$$

Taking into account (2.3a,b), (2.9) can be written as

$$\rho_f(1 + \beta_c^0 c) \left[\frac{\partial \mathbf{u}}{\partial t} + (\mathbf{u} \cdot \nabla)\mathbf{u} \right] = -\nabla p + \eta(c)\Delta\mathbf{u} + \rho_f(1 + \beta_c^0 c)\mathbf{g} + \mu_0 M_{sf}(\hat{H}) \frac{c}{c_0} \nabla H. \quad (2.15)$$

Let us consider an initial situation when the concentration of particles is infinitely small and the magnetic field is uniform everywhere. In this case, hydrostatic equilibrium is

provided by the equality

$$\nabla p^0 = \rho_f g. \tag{2.16}$$

As a result, the deviation from the initial state, described by the variables \mathbf{u} , p' , c , will be described by the equation

$$\rho_f(1 + \beta_c^0 c) \left[\frac{\partial \mathbf{u}}{\partial t} + (\mathbf{u} \cdot \nabla) \mathbf{u} \right] = -\nabla p' + \nu \Delta \mathbf{u} + \rho_f \beta_c^0 c g + \mu_0 M_S \frac{c}{c_0} f(\hat{H}) \nabla H. \tag{2.17}$$

To pass from natural variables to new variables, the streamfunction and vorticity, we divide equation (2.11) by $\rho_f(1 + \beta_c^0 c)$ and apply the curl operator to the resulting equation. Consider the transformation of this equation term by term. Since, in the case of two-dimensional motion, the vorticity has only one component ω directed perpendicular to the plane xy , the equation becomes scalar. The left side takes the standard form

$$\frac{\partial \omega}{\partial t} + (\mathbf{u} \cdot \nabla) \omega. \tag{2.18}$$

The term with pressure disappears because $\nabla \times \nabla \equiv 0$, and

$$\left. \begin{aligned} \nabla \times \left[\frac{\beta_c^0 c g}{(1 + \beta_c^0 c)} \right] &= -\frac{\partial}{\partial x} \left(\frac{\beta_c^0 c g}{(1 + \beta_c^0 c)} \right) \mathbf{e}_z = -\frac{\beta_c^0 g}{(1 + \beta_c^0 c)^2} \frac{\partial c}{\partial x} \mathbf{e}_z, \\ \nabla \times \left[\frac{\nu_0 \eta_r(c)}{(1 + \beta_c^0 c)} \Delta \mathbf{u} \right] &= \nu_0 \nabla \times [G(c) \Delta \mathbf{u}] = \nu_0 \frac{\partial G}{\partial c} \left(\frac{\partial c}{\partial x} \Delta u_y - \frac{\partial c}{\partial y} \Delta u_x \right) \mathbf{e}_z + \nu_0 G(c) \Delta \omega \mathbf{e}_z \end{aligned} \right\} \tag{2.19}$$

where $\eta_r(c) = \eta(c)/\eta_0$, $\nu_0 = \eta_0/\rho_0$, $G(c) = \eta_r(c)/(1 + \beta_c^0 c)$, \mathbf{e}_z is the unit vector directed along the z axis and index '0' refers to the base fluid.

As we use streamfunction–vorticity variables, we can rewrite the expression in the round brackets as $(\partial c/\partial x)(\partial \omega/\partial x) + (\partial c/\partial y)(\partial \omega/\partial y)$. Outside the diffusion front, the derivatives of the concentration are equal to zero and this term vanishes. Since we are interested in the instability of a flat horizontal diffusion front, and the structure of the flow in the area of the diffusion front is such that the streamlines are normal to the diffusion front, we can say that, on the one hand, in the diffusion front $\partial \omega/\partial y \rightarrow 0$, on the other hand, $\partial c/\partial x \rightarrow 0$. Thus, this term is equal to zero outside the diffusion front and goes to zero in the diffusion front. We neglect the first term on the right side of the last equation, and assume further

$$\nabla \times \left[\frac{\nu_0 \eta_r(c)}{(1 + \beta_c^0 c)} \Delta \mathbf{u} \right] = \nu_0 G(c) \Delta \omega \mathbf{e}_z. \tag{2.20}$$

The last term in the equation of motion (2.11) has the form

$$\nabla \times \left[\frac{\mu_0 M_S}{\rho_f c_0} \frac{c}{1 + \beta_c^0 c} f(\hat{H}) \nabla H \right] = \frac{\mu_0 M_S}{\rho_f c_0} \frac{f(\hat{H})}{(1 + \beta_c^0 c)^2} \left(\frac{\partial c}{\partial x} \frac{\partial H}{\partial y} - \frac{\partial c}{\partial y} \frac{\partial H}{\partial x} \right) \mathbf{e}_z. \tag{2.21}$$

Then the final equation of motion can be written in the form

$$\frac{\partial \omega}{\partial t} + (\mathbf{u} \cdot \nabla) \omega = G(c) \Delta \omega - \frac{\beta_c^0 g}{(1 + \beta_c^0 c)^2} \frac{\partial c}{\partial x} + \frac{\mu_0 M_S}{\rho_f c_0} \frac{f(\hat{H})}{(1 + \beta_c^0 c)^2} \left(\frac{\partial c}{\partial x} \frac{\partial H}{\partial y} - \frac{\partial c}{\partial y} \frac{\partial H}{\partial x} \right). \tag{2.22}$$

This equation is made dimensionless with the following variables: $\hat{t} = t/(h_1^2/D_0)$, $\hat{\omega} = \omega/(D_0/h_1^2)$, $\hat{u} = u/(D_0/h_1)$, $\hat{\psi} = \psi/D_0$, $\hat{H} = H/M_S$, where h_1 is the reference quantity

for the length, and D_0 is the diffusion coefficient as $c \rightarrow 0$. Then the system of equations can be written in dimensionless form as follows (any special symbols for dimensionless values are omitted):

$$\frac{1}{Sc} \left[\frac{\partial \omega}{\partial t} + (\mathbf{u} \cdot \nabla) \omega \right] = G(c) \Delta \omega - Ra \frac{1}{(1 + \beta_c^0 c)^2} \frac{\partial c}{\partial x} + Ra_m \frac{f(H)}{(1 + \beta_c^0 c)^2} \left(\frac{\partial c}{\partial x} \frac{\partial H}{\partial y} - \frac{\partial c}{\partial y} \frac{\partial H}{\partial x} \right), \quad (2.23)$$

where all variables are dimensionless, $Ra = \beta_c^0 g h_1^3 / (\nu_0 D_0)$, $Ra_m = \mu_0 M_S^2 h_1^2 / (\eta_0 D_0 c_0)$, $Sc = \nu_0 / D_0$.

Following the logic of the paper (Erglis *et al.* 2013), we will choose the reference length in a such way that $Ra = 1$, i.e. $h_1 = (\nu_0 D_0 / \beta_c^0 g)^{1/3}$. Then the final equation of motion takes the form

$$\frac{1}{Sc} \left[\frac{\partial \omega}{\partial t} + (\mathbf{u} \cdot \nabla) \omega \right] = \frac{\eta_r(c)}{1 + \beta_c^0 c} \Delta \omega - \frac{1}{(1 + \beta_c^0 c)^2} \frac{\partial c}{\partial x} + Ra_m \frac{f(H)}{(1 + \beta_c^0 c)^2} \left(\frac{\partial c}{\partial x} \frac{\partial H}{\partial y} - \frac{\partial c}{\partial y} \frac{\partial H}{\partial x} \right), \quad (2.24)$$

where the magnetic Rayleigh number is

$$Ra_m = \frac{\mu_0 M_S^2}{\rho_f c_0} [(\beta_c^0)^2 g^2 \nu_0 D_0]^{-1/3}. \quad (2.25)$$

In addition, the definition of vorticity $\omega = \nabla \times \mathbf{u}$ implies the equation for the streamfunction

$$\Delta \psi = -\omega. \quad (2.26)$$

On a microfluidic scale, the sedimentation of particles and magnetophoresis can be neglected (the external magnetic field is uniform), then the diffusion equation has the standard form

$$\frac{\partial c}{\partial t} + (\mathbf{u} \cdot \nabla) c = \nabla \cdot (D \nabla c). \quad (2.27)$$

Taking into account that the diffusion coefficient is inversely proportional to the viscosity of the liquid, which in turn depends on the concentration, we can write $D = D_0 / \eta_r(c)$ and the dimensionless diffusion equation takes the form (where $\eta_r(c) = \eta / \eta_0$)

$$\frac{\partial c}{\partial t} + (\mathbf{u} \cdot \nabla) c = \nabla \cdot \left[\frac{\nabla c}{\eta_r(c)} \right]. \quad (2.28)$$

The viscosity of the colloid depends on the concentration of particles. For low concentrations, the dependence of the viscosity of the suspension on the concentration of particles is described by Einstein's formula

$$\eta_r = 1 + 2.5c. \quad (2.29)$$

For high concentrations, a number of approximations are known that describe experimental data. This study uses the dependency (Vand 1948)

$$\eta_r = \exp \left(\frac{2.5c + 2.7c^2}{1 - 0.609c} \right). \quad (2.30)$$

The following conditions should be fulfilled at the container boundaries: no-slip condition for velocity, which means $\psi = 0$, $\partial \psi / \partial n = 0$, $\omega = -\partial^2 \psi / \partial n^2$ zero mass

Parameter	Carrier fluid			
	n-heptane (Berkovsky <i>et al.</i> 1993)	Transformer oil (Berkovsky <i>et al.</i> 1993)	Water (Erglis <i>et al.</i> 2013)	Experiment, kerosene, present paper
M_S , kA m ⁻¹	16.5	13.5	10.0	44.0
ρ , kg m ⁻³	941	1048	1077	1484
c_0	0.13	0.10	0.05	0.39
β_c^0	2.80	1.95	1.60	1.60
η , Pa s	5.20×10^{-4}	2.94×10^{-2}	1.14×10^{-3}	1.45×10^{-2}
η/η_0	1.9	1.4	1.14	9.7
$\eta_r(c_0)$	1.52	1.33	1.139	6.01
D_0 , m ² s ⁻¹	1.21×10^{-11} *	2.13×10^{-13} *	5.5×10^{-12} **	2.0×10^{-11} **
Ra_m	242 000	216 000	236 000	296 000
Sc	3.30×10^4	1.10×10^8	1.82×10^5	9.62×10^4
h_1 , m	5.60×10^{-7}	6.43×10^{-7}	7.05×10^{-7}	1.19×10^{-6}
t_1 , time corresponding to 1 s	38.5	0.516	11.0	14.2

Table 1. Physical properties of magnetic fluids: * denotes estimation on the basis of viscosity of (Erglis *et al.* 2013), ** denotes experiment.

flow for concentration $\partial c/\partial n = 0$; condition of magnetic field uniformity at the outer boundaries of the considered area $\partial F/\partial y = H_0$, $\partial F/\partial x = 0$; and conditions (2.5a,b) at the container boundaries.

3. Characteristic values of physical quantities and dimensionless parameters

Table 1 presents the dimensionless parameters for several typical magnetic fluids, the properties of which are presented in Berkovsky *et al.* (1993), Erglis *et al.* (2013) and our experimental data. The diffusion coefficient for a water-based magnetic fluid corresponds to Erglis *et al.* (2013), and for fluids from Berkovsky *et al.* (1993) is calculated on the assumption that it is inversely proportional to the viscosity.

As you can see, the physical properties of magnetic fluids differ significantly. For example, the viscosity of fluids based on transformer oil and n-heptane differs by three orders of magnitude. However, the Rayleigh magnetic numbers for all fluids are in the range of 200 000–300 000. The reference length h_1 is in the range of 0.6–1.2 μm . Let us recall that it is this quantity that is used as a reference value for length in the dimensionless system of equations. Since the characteristic size for microfluidics devices is approximately 100 μm , then, taking into account the value of h_1 , all numerical simulations were carried out for a dimensionless cavity height of 100. Magnetic susceptibility of the fluid in almost all simulations is equal to $\chi_0 = 2$.

4. Numerical solution method

4.1. Mesh

A rectangular mesh was constructed in the calculation domain (figure 1). The mesh was uniform along the vertical coordinate y in the container with the number of segments N_y . The number of segments between the container and the poles is Nd both above and below the container. Along the horizontal coordinate x the mesh was uniform within

the container. Outside the container, the length of the first segment was equal to the segment in the container, and then increased exponentially with the coefficient 1.05. The number of segments in the container is N_x , and outside it is $N_r -$ both on the right and on the left. In all simulations, $N_r = 30$, $N_d = 10$, N_x and N_y were selected depending on the problem.

4.2. Method

The problem was solved numerically by the finite volume method (Patankar 1980). In accordance with this method, differential equations (2.4), (2.12), (2.14) and (2.15) are presented as

$$\frac{\partial \omega}{\partial t} = \nabla \cdot \mathbf{J}_\omega + F_\omega; \quad \frac{\partial c}{\partial t} = \nabla \cdot \mathbf{J}_c; \quad \nabla \cdot \mathbf{J}_F = 0; \quad \nabla \cdot \mathbf{J}_\psi = -\omega, \quad (4.1a-d)$$

where

$$\mathbf{J}_\omega = Sc\eta_r(c)\nabla\omega - \mathbf{u}\omega; \quad \mathbf{J}_c = \nabla c/\eta_r(c) - \mathbf{u}c; \quad \mathbf{J}_F = \mu\nabla F; \quad \mathbf{J}_\psi = \nabla\psi, \quad (4.2a-d)$$

and then replaced by integral equations on a finite volume surrounding each grid node

$$\left. \begin{aligned} \int_\Omega \frac{\partial \omega}{\partial t} d\Omega &= \oint_L \mathbf{J}_\omega \cdot \mathbf{n} dl + \int_\Omega F_\omega d\Omega; & \oint_L \mathbf{J}_\psi \cdot \mathbf{n} dl &= - \int_\Omega \omega d\Omega; \\ \int_\Omega \frac{\partial c}{\partial t} d\Omega &= \oint_L \mathbf{J}_c \cdot \mathbf{n} dl; & \oint_L \mathbf{J}_F \cdot \mathbf{n} dl &= 0 \end{aligned} \right\}. \quad (4.3)$$

Here, Ω is the control volume surrounding the node. In two dimensions, the volume is actually the area, and L is the closed line bounding the area.

To approximate these integral equations, we must assume some kind of interpolation function for the variables ω , ψ , c , F . Following Patankar (1980), we use linear functions for ψ and F and exponential functions for ω and c between the central node of the control volume and the neighbour node:

$$\left. \begin{aligned} \omega &= A_\omega \exp \left[\frac{u_x x + u_y y}{Sc\eta_r(c)} \right] + B_\omega, \\ c &= A_c \exp[\eta_r(c)(u_x x + u_y y)] + B_c, \\ \psi &= A_\psi x + B_\psi y + C_\psi; \quad F = A_F x + B_F y + C_F \end{aligned} \right\}, \quad (4.4)$$

and all coefficients are determined for each boundary line of the control volume separately through the central node and nearest outside node.

The advantage of the exponential scheme is that interpolation function is the exact solution of the equation without the force term and it provides high accuracy for both small and large advective fluid velocities. At low velocities, this method turns into a central difference method, and at high velocities, it turns into an upwind method. This advantage is important for the non-stationary problem in our case, since at the beginning of the process the intensity of the advective velocities is very large, but over time the velocities decrease.

Implicit method is employed for time discretization of the concentration and the vorticity equations. The convergence criteria for residuals in solving the Laplace equation for the magnetic potential F and the Poisson equation for the streamfunction ψ are considered as 10^{-7} .

Since the range of values of dimensionless criteria that determine the system of equations is very wide, the time step in each case decreased until time step independence

was ensured. In any case, it was $\Delta t = \Delta x \Delta y / k$, and k was in the range from 4×10^4 to 5×10^6 .

At the initial moment of time, random perturbations with an amplitude of $0.0005c_0$ were set on the upper grid line with a concentration of c_0 (for example, $y_0 = 0.25$). Thus, the initial smearing is equal to one step of the grid in the numerical simulation.

4.3. Validation of the code

4.3.1. Diffusion in the absence of a magnetic field

The one-dimensional diffusion problem

$$\frac{\partial c}{\partial t} = D \frac{\partial^2 c}{\partial y^2}, \tag{4.5}$$

with the initial condition as the Heaviside step function $c(x, 0) = c_0 H(y - y_0)$, where y_0 is the initial position of the diffusion front, has the exact solution. This solution is described by the error function and looks like (for dimensionless equation $D = 1$)

$$c(y, t) = \frac{c_0}{2} \left[1 - \Phi \left(\frac{y - y_0}{2\sqrt{t}} \right) \right], \quad \Phi(z) = \frac{2}{\sqrt{\pi}} \int_0^z e^{-\mu^2} d\mu. \tag{4.6a,b}$$

It seems that, in the absence of a magnetic field ($H = 0, Ra_m = 0$), the problem described corresponds well to the one-dimensional formulation. As a test problem, the container $L_x = 500, L_y = 100, h = 25$ is considered. The mesh $N_x \times N_y = 250 \times 50$ is used. The ratio of the length of the layer of magnetic fluid to its thickness is 20:1 and edge effects should not play a significant role (moreover, the width of the dimensionless diffusion front $s = \delta/h_1$ in the numerical procedure at the initial moment is equal to one step of the mesh $s = \Delta y = 2$). But (2.28) differs significantly compared to (4.5). Moreover, at the initial moment, a random concentration perturbation with an amplitude of $0.0005c_0$ is set along the magnetic/non-magnetic fluid interface, which due to the gravity causes the fluid to move. This movement can affect the diffusion process.

In order to better understand, is it possible to compare the solution of (2.24), (2.26) and (2.28) in the case of the absence of a magnetic field with the solution of (4.5). We will see how flow in the container changes in time after the two fluids come in contact and compare the advective and diffusive fluxes. Let $c_0 = 0.34, Sc = 10^5, Ra_m = 0, H = 0$ (the selected values of the parameters are discussed below). Note that, because within the control volume method the value of the variable within the entire control volume is equal to the value at the node, and since the initial concentration is $c_0 = 0.34$ at all nodes in the range from $y = 0$ to $y = 24$, the initial position of the diffusion front $y_0 = 24 + \Delta y / 2 = 25$.

Figure 2 shows that the maximum value of the streamfunction first increases rapidly and then gradually decreases. The largest value is achieved at $t = 8$ and is equal to $\psi_{max} = 4.07 \times 10^{-4}$. In this case, as can be seen from figure 3, the width of the diffusion front is approximately $s = 5$. Then the ratio of advective mass flux and diffusion flux can be estimated. In (2.15), the term responsible for the advective mass flow has the form $(\mathbf{u} \cdot \nabla)c$ and its maximum value can be estimated as $\partial\psi/\partial y \cdot \partial c/\partial y \sim \psi_{max}/s^2$. The term responsible for the diffusion mass transfer is of the order of $\Delta c \sim c/s^2$. The ratio of these quantities is $\psi_{max} \sim 10^{-4}$. Thus, without a magnetic field, diffusion fluxes are four orders of magnitude larger than advective ones, and the solution to (2.28) can be compared with the solution (4.6a) to (4.5).

The structure of the diffusion front at time $t = 9.306$ for the case $\eta_r(c) = 1$ is shown in figure 4. As can be seen, the obtained numerical solution of the two-dimensional problem

Instability of diffusion front of miscible magnetic fluid

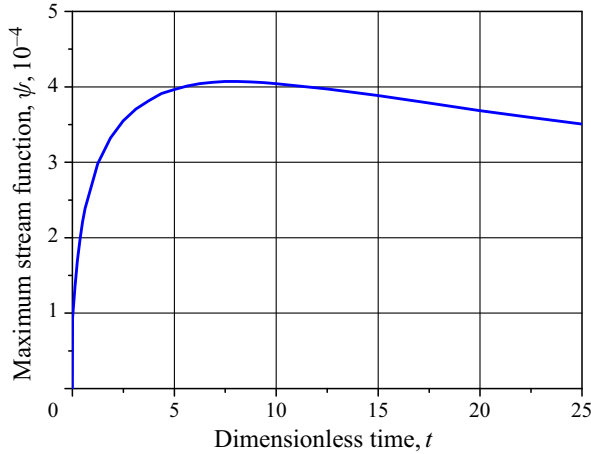


Figure 2. Maximum streamfunction vs time for $\Delta t = 6.25 \times 10^{-6}$, $H = Ra_m = 0$, $\eta_r(c) \neq 1$, $Sc = 10^5$.

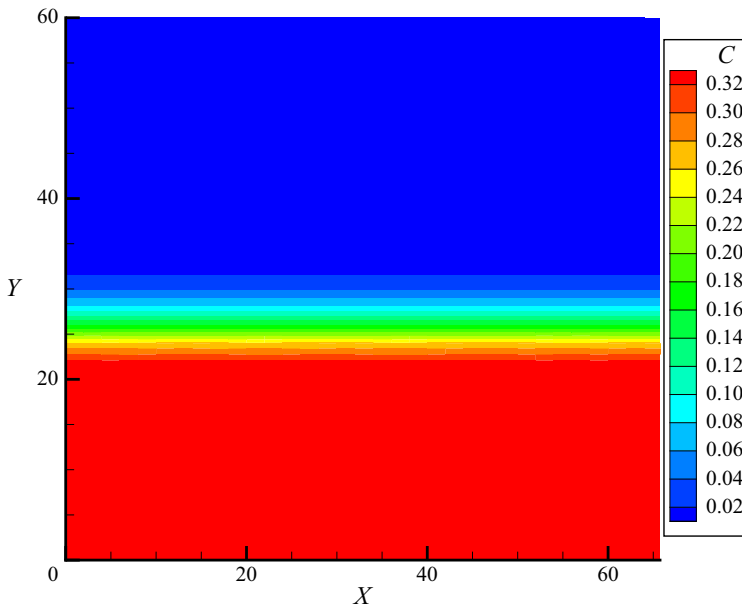


Figure 3. The diffusion front at the moment $t = 8$ for $\Delta t = 6.25 \times 10^{-6}$, $c_0 = 0.34$, $H = Ra_m = 0$, $\eta_r(c) \neq 1$, $Sc = 10^5$. Here and in all the figures below, the numbers under the part of the chamber are dimensionless coordinates in h_1 units.

fits well with the solution of the classical one-dimensional problem. This indicates that the mass transfer due to advective flows, in this case, is really much less than the diffusion transfer, and validated that the method and code are rather reliable. Note that, as given in figure 4, the concentration distribution corresponds to all values of the x coordinate, i.e. the diffusion front remains flat.

The results presented in figure 4 are obtained for $\eta_r(c) = 1$, but the dependence of the viscosity on the concentration of magnetic particles can be significant for highly concentrated fluids and for a large time. In fact, for the time $t = 7.031$ we see the difference

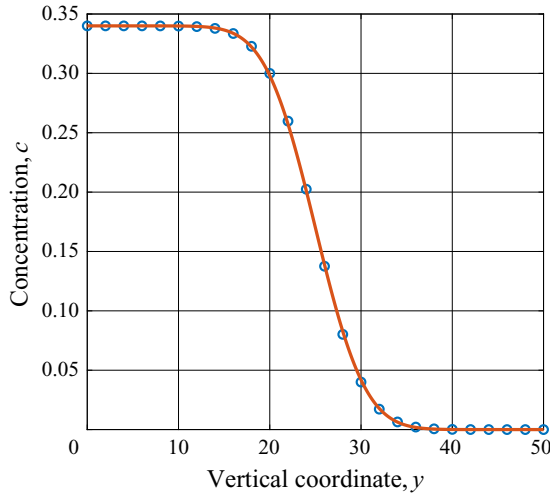


Figure 4. Concentration as a function of vertical coordinate for $\Delta t = 1.3 \times 10^{-6}$, $t = 9.306$, $H = Ra_m = 0$, $\eta_r(c) = 1$, $Sc = 10^5$. Here, solid line is from (4.6a), and markers are from the numerical solution of (2.24), (2.28).

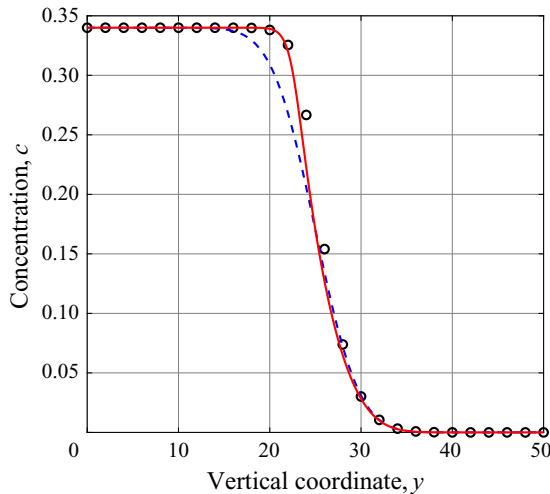


Figure 5. Concentration as a function of vertical coordinate for $\Delta t = 1.3 \times 10^{-6}$, $t = 7.031$. $H = Ra_m = 0$, $Sc = 10^5$, $\eta_r(c) \neq 1$. Here, dashed line is from (4.6a), solid line from (4.7), and markers are from the numerical solution of (2.24), (2.28).

between the numerical results taking into account $\eta_r(c)$ and the analytical solution (4.6a) (dashed line) in the rear part of the diffusion front (figure 5). Since the reference value for dimensionless time is the diffusivity, which is related to the concentration as $D = D_0/\eta_r(c)$, the solution (4.6a) can be rewritten as

$$c(y, t) = \frac{c_0}{2} \left[1 - \Phi \left(\frac{y - y_0}{2\sqrt{t/\eta_r(c)}} \right) \right]. \quad (4.7)$$

The concentration is on both the left and right sides of (4.7). Distribution of the concentration over the diffusion front, obtained after solving this equation numerically

Instability of diffusion front of miscible magnetic fluid

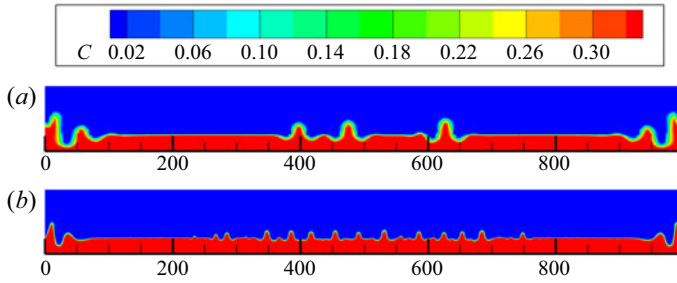


Figure 6. The initial stage of the instability of the diffusion front for $Sc = 10\,000$, $Ra_m = 158\,800$, $H = 1$, $k = 6.4 \times 10^4$, $c_0 = 0.34$: (a) $N_x = 200$, $N_y = 40$; (b) $N_x = 1600$, $N_y = 400$.

$N_x \times N_y$	λ
200×50	52.6
200×100	50.0
400×200	43.5
800×200	31.3
800×300	22.2
1200×300	18.2
1200×400	18.2
1600×400	17.9

Table 2. Dependence of the wavelength of unstable disturbances on the number of grid nodes.

by an iterative method for every y , is shown in [figure 5](#) as a solid line. This line and the numerical results are matched very well.

A high level of mass conservation of the numerical method should be noted too: for 4×10^6 time steps, the average concentration in the container volume changed from $\bar{c} = 9.121 \times 10^{-2}$ to $\bar{c} = 9.381 \times 10^{-2}$.

4.3.2. Diffusion in the magnetic field

As seen from [figures 4](#) and [5](#), even a rather coarse grid of 50×250 nodes in a container with an aspect ratio of 1 : 5 allows one to calculate the expansion of a flat diffusion front with high accuracy. However, in the presence of a magnetic field, the diffusion front ceases to be flat and the parameters of the mesh must be determined additionally. In addition, due to the distortion of the magnetic field near the side boundaries of the container, edge effects can significantly affect the shape of the diffusion front. Therefore, test simulations were carried out for an aspect ratio of the container 1 : 10 and the thickness of the magnetic fluid layer at a quarter of the container height. As seen from [figure 6](#), the distance between adjacent bends of the diffusion front line (the wavelength of the most unstable disturbances λ) depends significantly on the number of grid nodes. [Table 2](#) shows that reliable data for the instability simulation can be obtained using a mesh with a number of nodes of at least 1200×300 , which corresponds to a distance between nodes along the x -axis of no more than $h_x = 1000/1200 = 0.83$ and a distance between nodes along the vertical axes $h_y = 100/300 = 0.33$. In further simulations, grids with $h_x = 0.5$ and $h_y = 0.33$ were used.

5. Numerical results and discussion

5.1. Process of the instability development

The main parameters affecting the change in the shape of the diffusion front are the magnitude of the magnetic field H , the properties of the liquid described by the magnetic Rayleigh number Ra_m and the Schmidt number Sc , the thickness of the magnetic fluid layer h and the width of the diffusion front s at the moment of turning on the magnetic field. Before revealing the nature of the influence of each of these factors on the onset of instability of the diffusion front and the nature of this instability, let us consider how this instability develops in magnetic fields of various magnitudes.

In [figure 7](#) it can be seen that, at first, the line of separation of the magnetic and non-magnetic media near the side boundaries of the container changes due to edge effects associated with the non-uniformity of the magnetic field in these regions. Then, wave-like distortion of the flat surface occurs along the entire part of the diffusion front, which previously remained flat. Further, these disturbances grow in amplitude without changing their position. Particular attention should be paid to the fact that, as in a real physical experiment, in a numerical experiment, the distances between neighbouring peaks are not strictly equal. The ratio of the standard deviation to the mean value of this distance (the distances between the peaks located at a distance of approximately 200 from the container edges were excluded from the calculation) varied for various parameters of the problem in the range from 15 % to 26 %. As will be seen from the data presented below, this value is the higher the greater the magnetic field.

The mechanism of development of instability is shown in [figure 8](#), which shows the streamlines in the container at the same moments of time as in [figure 7](#). At time $t = 7.0$, the diffusion front remains flat everywhere, with the exception of regions close to the edges of the container. However, as can be seen from [figure 8\(a\)](#), by this time, a system of vortices had already formed, the distance between which determines the distance between the subsequently appearing peaks. As the formation of edge peaks ends, the intensity of the vortices near the lateral boundaries, as can be seen from [figure 8\(c\)](#), falls, while the vortices under the central part grow. The amplitude of the peaks at the diffusion front also increases. This process continues as the peaks grow. Note that, based on [figures 7](#) and [8](#), it can be concluded that the region of influence of edge effects at a given value of the magnetic field extends approximately to a distance of 200, i.e. eight layer thickness.

As can be seen from [figures 7](#) and [8](#), the periodic structure of vortices ([figure 8a](#)) is formed much earlier than visible distortions are formed at the diffusion front ([figure 7b](#)). The time at which distortions appear on the diffusion front line depends on the force action from the magnetic field and is determined by the $K_H = f(H)HRa_m$ complex. Simulation for the aspect ratio of 1 : 15, $L_y = 100$, $h = 25$, $Sc = 10^5$ shows that this dependence has a power-law character ([figure 9](#)), and is close to inversely proportional. The issue of the critical value of the parameter K_H and its dependence on the parameters of the problem is not clear and is the subject of particular research.

Instability develops somewhat differently at high magnetic fields. As seen from [figure 10](#), the edge peaks grow so rapidly that this process, spreading from the edges to the centre, gradually covers the entire container ([figure 10a–f](#)). However, the distance between adjacent peaks in the central part of the container is still somewhat smaller than at the edges. Attention is drawn to the fact that, after the primary peaks have formed, smaller satellites appear between them ([figure 10g–j](#)). Their occurrence is associated with a complex flow structure between the main peaks. An upward flow forms in the centre of the main peaks, and a downward one forms along the diffusion front on the outer side of the peaks. This downward flow, reaching the bottom of the container, breaks up into

Instability of diffusion front of miscible magnetic fluid

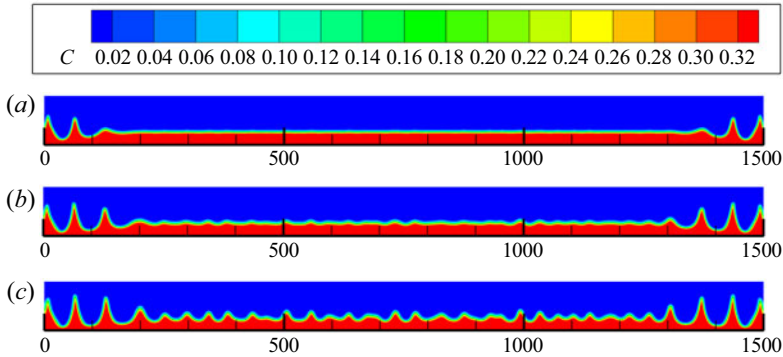


Figure 7. Change in the shape of the diffusion front in time for $c_0 = 0.34$, $H = 0.021$, $Ra_m = 158\,800$, $Sc = 10^5$, $K_H = f(H)HRa_m = 137$, $L = 1500$, $l = 100$, $h = 25$, $N_x = 3000$, $N_y = 300$, $\Delta t = 2.598 \times 10^{-4}$: (a) $t = 7.0$; (b) $t = 9.33$; (c) $t = 10.89$.

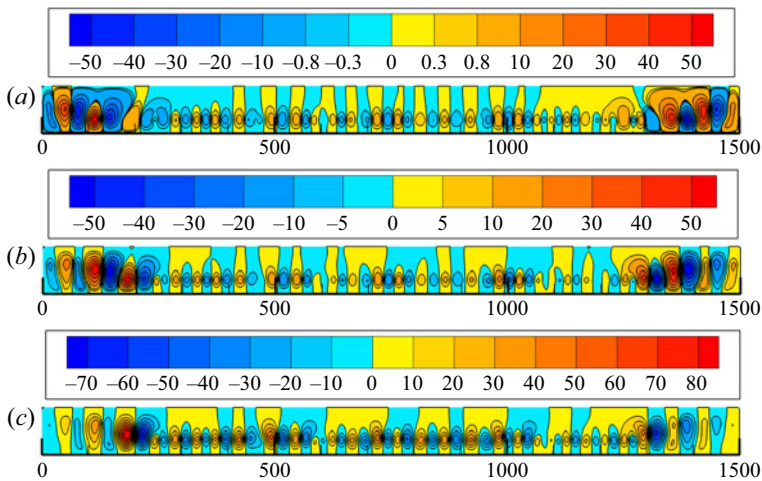


Figure 8. Isolines of the streamfunction $\psi = \text{const}$ for $c_0 = 0.34$, $H = 0.021$, $Ra_m = 158\,800$, $Sc = 10^5$, $K_H = f(H)HRa_m = 137$, $L_x = 1500$, $L_y = 100$, $h = 25$, $N_x = 3000$, $N_y = 300$, $\Delta t = 2.598 \times 10^{-7}$: (a) $t = 7.0$; (b) $t = 9.33$; (c) $t = 10.89$.

secondary flows and is the cause of the appearance of numerous secondary vortices. As a result, as can be seen from figure 10(*i, j*), between the main peaks, the occurrence of one, two or three additional peaks is possible. Over time, these peaks disappear as a result of diffusion–advective mixing of fluids.

The dynamics of the development of the instability of the diffusion front is demonstrated by the animation obtained as a result of numerical simulation, attached to this paper. This animation was obtained for the following problem parameters: $c_0 = 0.05$, $H = 0.054$, $Ra_m = 200\,000$, $Sc = 170\,000$. These parameters, as far as possible, correspond to the experimental conditions (Erglis *et al.* 2013). The aspect ratio of the container was 1 : 15, the height of the container was $L_y = 150$, the thickness of the magnetic fluid layer was $h = L_y/4$, the number of nodes during the numerical simulation was $N_x \times N_y = 4500 \times 450$. Table 1 shows that the reference value for the length is $h_1 = 0.705\ \mu\text{m}$, i.e. the container height $L_y = 150$ approximately corresponds to the experimental value $L_y = 127\ \mu\text{m}$. In this case, the average distance between adjacent peaks in the

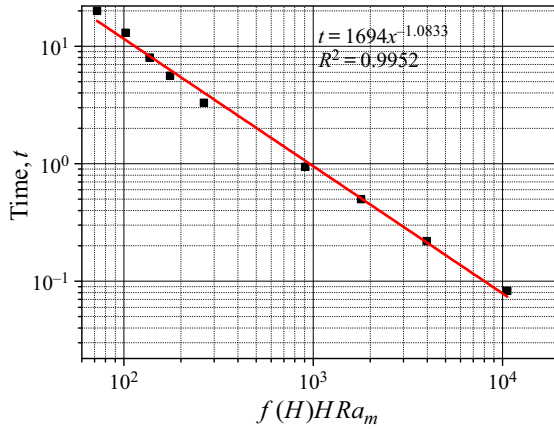


Figure 9. Time of the instability development vs the magnetic complex $K_H = f(H)HRa_m$ for $c_0 = 0.34$, $Sc = 10^5$, $L_x = 1500$, $L_y = 100$, $h = 25$, $N_x = 3000$, $N_y = 300$, $\Delta t = 2.598 \times 10^{-7}$.

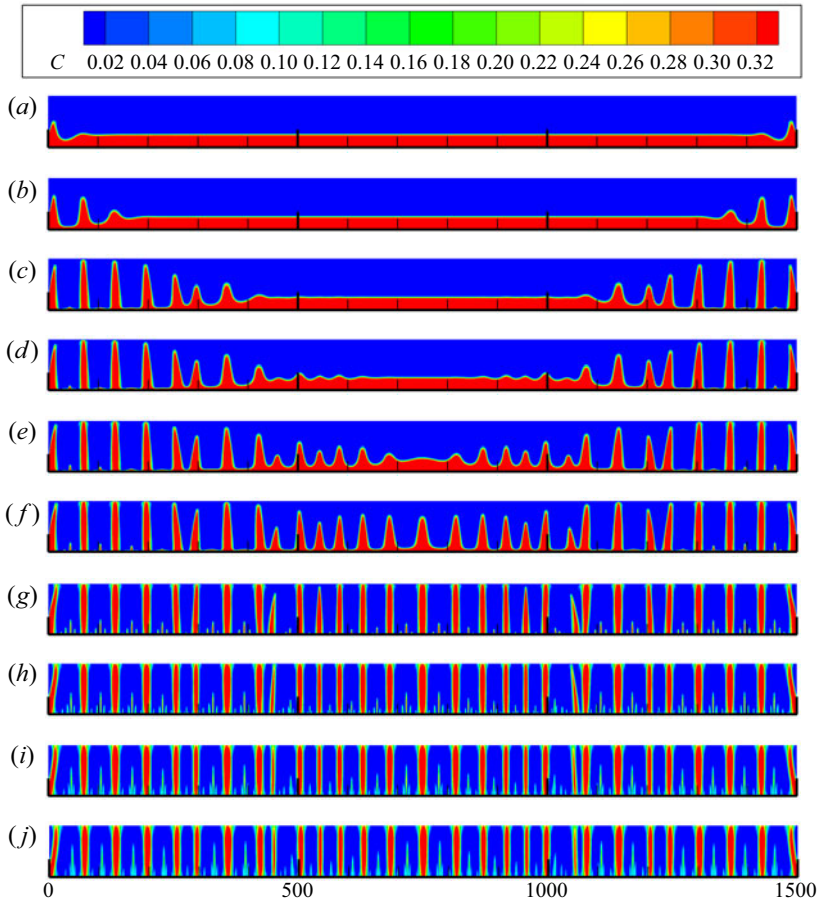


Figure 10. Development of instability in a high magnetic field for $c_0 = 0.34$, $H = 0.5$, $Ra_m = 10^5$, $Sc = 10^5$, $K_H = f(H)HRa_m = 25\,000$, $L_x = 1500$, $L_y = 100$, $h = 25$, $N_x = 3000$, $N_y = 300$, $\Delta t = 2.598 \times 10^{-7}$: (a) $t = 2.59 \times 10^{-2}$; (b) $t = 4.68 \times 10^{-2}$; (c) $t = 9.88 \times 10^{-2}$; (d) $t = 0.108$; (e) $t = 0.125$; (f) $t = 0.148$; (g) $t = 0.260$; (h) $t = 0.546$; (i) $t = 1.092$; (j) $t = 1.559$.

Sc	$\langle \lambda \rangle$	σ	$\sigma / \langle \lambda \rangle$
5000	19.61	4.00	20.4 %
10 000	19.03	4.90	25.8 %
20 000	19.11	4.32	22.6 %
40 000	20.31	3.62	17.8 %
80 000	19.90	3.73	18.8 %

Table 3. Average wavelength versus Schmidt number.

numerical simulation is 65, i.e. 46 μm , while in the experiment (Erglis *et al.* 2013) a value of approximately 20 μm was obtained. However, as will be shown below, the wavelength of unstable perturbations depends significantly on the thickness of the magnetic fluid layer and, with its decrease, can decrease by a factor of 3–5. Since the thickness of the magnetic fluid layer in the experiment (Erglis *et al.* 2013) is unknown, an exact comparison with experimental data is impossible.

5.2. The influence of the Schmidt number

Equation (2.24) shows that the Schmidt number is included only in the non-stationary part of the equation and, therefore, should not affect the critical values of the wavelength, which are determined by setting the equality of the right side of this equation to zero. However, we checked this statement for the case of moderate magnetic fields: $H = 0.125$, $Ra_m = 158\,800$ and cavity of size $L_x = 1000$, $L_y = 100$. The data are presented in table 3. Here, $\langle \lambda \rangle$ is the average wavelength without taking into account the edge sections, σ is the standard deviation. It can be seen that, within the error limits, the wavelength of unstable perturbations is indeed practically independent of the Schmidt number. In further simulations, the Schmidt number is assumed to be 100 000, which corresponds to the typical physical properties of magnetic fluids presented in table 1.

5.3. Influence of the magnetic field on the wavelength

One of the main parameters determining the development of the instability of the contact line of magnetic and non-magnetic fluids (both miscible and immiscible) is the magnitude of the magnetic field. To determine its influence, we set the following problem parameters: $Ra_m = 158\,800$, $Sc = 10^5$, $h = L_y/4$ and two options for container geometry: (i) $L_x = 1000$, $L_y = 100$, $N_x \times N_y = 2000 \times 300$; (ii) $L_x = 1500$, $L_y = 100$, $N_x \times N_y = 3000 \times 300$. Figure 11 shows that the results of both simulations are practically the same, i.e. the influence of edge effects is insignificant.

It is noteworthy that the wavelength decreases with increasing magnetic field, while the linear theory constructed in Erglis *et al.* (2013) for a layer of magnetic fluid of infinite depth predicts an increase in wavelength with increasing magnetic field; in fact it predicts the increase of wavelength of the fastest-growing mode, to be precise. The range of possible wavelengths increases with the field increase. The fact that bending of the diffusion front should be observed corresponding to perturbations with the fastest-growing wavelength is an assumption. This assumption is reasonable, but it is only an assumption. The reasons for this discrepancy are not clear, it could be, for example, differences in the formulations of the problems: the finite depth of the layer, the influence of the boundaries of the container, nonlinear effects or, most probably, the infinitesimal thickness of the

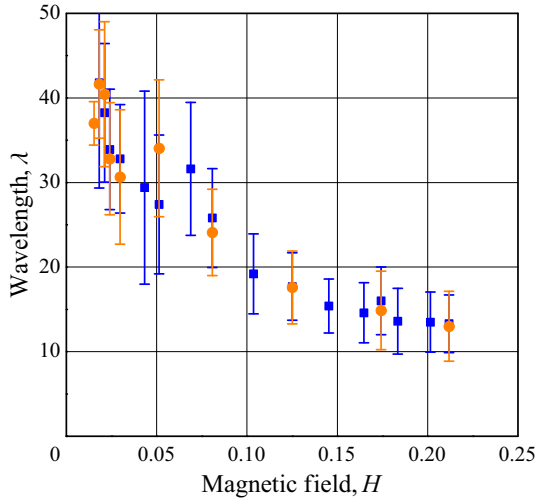


Figure 11. Dependence of the wavelength on the magnitude of the magnetic field. Squares, $L_x = 1000$; circles, $L_x = 1500$. Error bars show σ .

diffusion front in the linear theory. The last assumption is confirmed by the results of Cebers (1997), who for a close problem showed that smearing of the diffusion front shifts the most dangerous mode to a longer wavelength. The result obtained rather resembles the behaviour of the free interface of a magnetic fluid, on which the Rosensweig instability (Cowley & Rosensweig 1967) develops upon instantaneous switching on of a magnetic field of various magnitudes (Bashtovoi, Krakov & Reks 1985; Dikansky, Zakinyan & Mkrtchyan 2010; Zakinyan, Mkrtchyan & Dikansky 2016). With an increase in the value of the switched-on magnetic field, the length of the most rapidly developing wavelength in this case significantly decreased. This result was consistent with the linear theory, in which the dispersion equation is determined by both the magnitude of the magnetic field and the surface tension and thickness of the magnetic fluid layer. However, in the problem considered in this paper, there is no surface tension, so that direct analogies with the results of Bashtovoi *et al.* (1985), Dikansky *et al.* (2010) and Zakinyan *et al.* (2016) are impossible. We will return to the discussion of this analogy below.

In the simulations performed for $H \leq 0.015$, a wave-like distortion of the diffusion front was observed only near the side boundaries of the container (similar to figure 10a), the rest of the line of contact of the liquids remained flat throughout, while advective cells (similar to figure 8a) of very low intensity were observed which did not lead to surface distortion. Thus, it is obvious that there is a threshold value of the magnetic field below which the instability of the diffusion front is not observed. However, we cannot assert that this threshold value is 0.015, since, with a decrease in the magnetic field, the development of instability slows down and this leads to an increase in run time. For example, the run time in the case of $H = 0.015$ was more than three months and the process was stopped due to the low probability of detecting wave formation at the interface between the fluids.

5.3. Wavelength dependence on fluid properties

The influence of the properties of miscible magnetic and non-magnetic fluids is described by the Rayleigh magnetic number. Since the last term in (2.24), which is the source of advective flows, is proportional to both the magnetic field and the magnetic Rayleigh

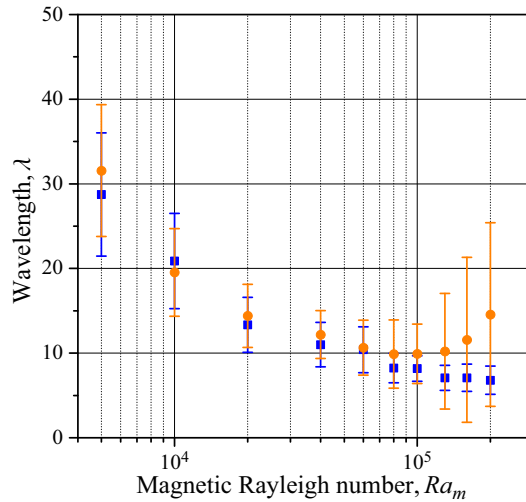


Figure 12. Wavelength dependence on the magnetic Rayleigh number. Squares, $L_x = 1000$; circles, $L_x = 1500$. Error bars show σ .

number, it can be expected that the $\lambda(Ra_m)$ dependence will be qualitatively similar to the $\lambda(H)$ dependence. The simulation was performed for the parameters $H = 0.5$, $Sc = 10^5$, in the range of values of the magnetic Rayleigh number from 5000 to 200 000. We used the same two options for the geometry of the container and the mesh as in the study of the dependence on the magnetic field. Indeed, figure 12 shows that the wavelength decreases with increasing magnetic Rayleigh number. However, since the magnetic field $H = 0.5$, chosen to cover the widest possible range of parameter values, is large, and at large Ra_m values, waves of different lengths simultaneously develop at the diffusion front, the spread of λ values in this case turns out to be much larger. The ratio $\sigma/\langle\lambda\rangle$ for $Ra_m > 130\,000$ reached 84 %, and this scatter is especially large in the case of $L_x/L_y = 15$.

5.4. Dependence of the wavelength on the complex parameter

Since the last term in (2.24), which is the source of advective motion, takes into account the nonlinear nature of the dependence of the magnetization on the magnitude of the magnetic field strength, i.e. is proportional not only to H , Ra_m , but also to $f(H)$, then a complex parameter $K_H = f(H)HRa_m$ can be introduced, which is their product. In the investigated range of parameters ($H < 0.5$, $Ra_m < 200\,000$, $102 < K_H < 50\,000$), all data are in good agreement with a single curve (figure 13).

5.5. The nature of the instability of the diffusion front

As in the development of Rosensweig's instability (Cowley & Rosensweig 1967; Bashtovoi *et al.* 1985; Dikansky *et al.* 2010; Zakinyan *et al.* 2016), which arises on the free surface of the magnetic fluid, peaks form at the diffusion front, the distance between them decreasing with increasing magnetic field. This can lead to the conclusion that the instability under study is a complete analogue of Rosensweig's instability. However, there are several fundamental differences between them. In the case of Rosensweig's instability, the wavelength of the most unstable perturbations is determined by the relation $\lambda = 2\pi\sqrt{\alpha/\Delta\rho g}$, where α is the surface tension, $\Delta\rho$ is the difference in the densities of

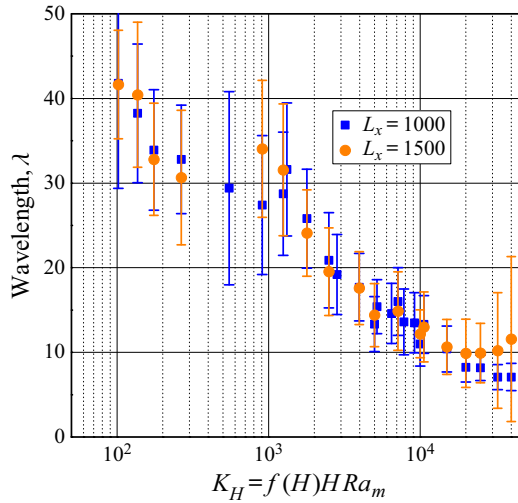


Figure 13. The dependence of the wavelength on the complex $K_H = f(H)HRa_m$. Squares, $L_x = 1000$; circles, $L_x = 1500$. Error bars show σ .

the contacting fluids. This wavelength, firstly, does not depend on the thickness of the magnetic fluid layer (Bashtovoi 1978) and, secondly, it increases with increasing surface tension α . Let us consider the influence of these factors for the instability under study.

The dependence on the layer thickness was investigated for the parameters corresponding to the magnetic fluid based on kerosene, for which the experiment was carried out described below (table 1): $Sc = 2.56 \times 10^5$, $Ra_m = 5.59 \times 10^5$, $\chi_0 = 2.4$, $c_0 = 0.41$, $H = 0.03$. The container has dimensions $L_x = 1000$, $L_y = 100$, the thickness of the magnetic fluid layer was 6.25, 12.50, 18.75, 25, 35, 50. The data presented in figure 14 show that, when the layer thickness is less than 18, the wavelength of unstable disturbances decreases from 30 to 14. It can be assumed that, perhaps, with a higher container height, the wavelength will also increase. However, we were unable to perform the corresponding simulations due to a significant increase in run time with increasing container size and the need to maintain the distance between nodes $h_x = 0.5$, $h_y = 0.3$ to ensure the accuracy of the simulations.

Simulation of the instability of a thin layer of liquid was also carried out, with properties corresponding to the data of Erglis *et al.* (2013) (table 1). In contrast to the version shown in the animation and discussed above, the thickness of the magnetic fluid layer was $h = 9$. In this case, the average wavelength was $\lambda = 26$, which is significantly lower than the value of 65 obtained for a layer with a thickness of 37. Note that the value of the wavelength $\lambda = 26$ for this liquid corresponds to the dimensional value of $26 \times 0.705 = 18.3 \mu\text{m}$, which practically coincides with the experimental data (Erglis *et al.* 2013).

It is usually assumed that there is no surface tension at the diffusion boundary of miscible fluids. However, there is a hypothesis of Korteweg (1901), who suggested that a non-uniform density (concentration or temperature) distribution leads to stresses in a fluid. Zeldovich (1949) considered the problem of an effective interfacial tension for such systems and derived an expression for this tension

$$\alpha = k \frac{(\Delta c)^2}{\delta}, \tag{5.1}$$

Instability of diffusion front of miscible magnetic fluid

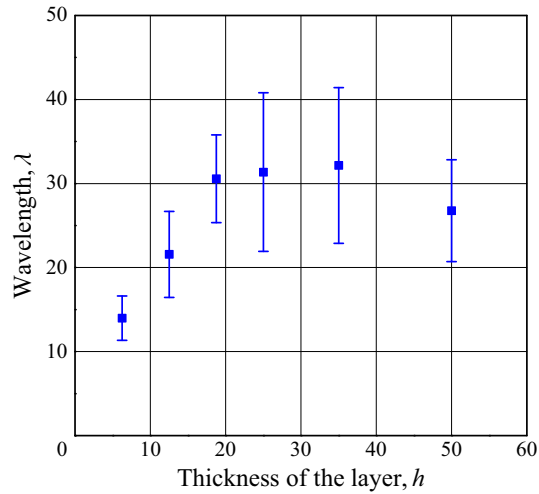


Figure 14. Average wavelength versus layer thickness. Error bars show σ .

where k is a system-specific parameter, Δc is the variation of mass fraction through the mixing zone and δ is the width of that zone. Although the coefficient k is unknown, the applicability of this hypothesis in the case of magnetic fluids is easy to assess. For highly concentrated microdroplet aggregates arising in a magnetic fluid (Bacri, Salin & Massart 1982; Ivanov 2019), the surface tension is estimated as $1.5 \times 10^{-7} \text{ N m}^{-1}$. The boundary of a microdroplet aggregate, in which the concentration of magnetic particles is almost two orders of magnitude higher than in the surrounding fluid, can be considered to be similar to the diffusion front. Since the concentration of particles in a magnetic fluid is lower than in micro-droplet aggregates, the surface tension (if it exists) can be estimated as $\alpha \sim 10^{-7} \text{ N m}^{-1}$. Since the difference between the densities of the magnetic fluid and the base fluid can be considered equal to $\Delta \rho \sim 100 \text{ kg m}^{-3}$, the wavelength when Rosensweig's instability occurs should be equal to $\lambda = 2\pi\sqrt{\alpha/\Delta\rho g} \approx 60 \text{ }\mu\text{m}$. Obviously, in order of magnitude, this value corresponds to both experimental data and our simulations, so that an analogy with Rosensweig's instability can be considered as possible.

However, according to the Korteweg–Zel'dovich hypothesis, with an increase in the width of the diffusion layer δ the effective surface tension coefficient α should decrease. Then, if the analogy with Rosensweig's instability is valid, the wavelength of unstable perturbations $\lambda = 2\pi\sqrt{\alpha/\Delta\rho g}$ should also decrease. To analyse this situation, an instability simulation was performed for the following parameter values: $H = 0.5$, $Ra_m = 10^5$, $Sc = 10^5$, $\chi_0 = 2$, $c_0 = 0.34$, $L_x = 1500$, $L_y = 100$, $h = 25$, $h_x = 1/2$, $h_y = 1/3$. At the initial moment of time, the concentration distribution along the y coordinate was specified in accordance with expression (4.6a) for the moments of time $t = 0.001, 0.010, 0.016, 0.036, 0.600, 0.700, 0.920, 2.0, 3.0, 4.0, 6.0, 20.0$. Note that, for fluids with moderate viscosity (water, kerosene), as can be seen from table 1, even the maximum time $t = 20$ corresponds to several seconds of contact time of the miscible magnetic and non-magnetic fluids. The diffusion front width was calculated as the distance between points with a concentration of 0.339 and 0.001. This width was, corresponding to the values of t , the following values: 0.30, 0.78, 1.50, 3.0, 4.5, 6.0, 7.5, 11.0, 13.4, 15.5, 19.0, 34.8. Figure 15 shows that, with an increase in the initial width of the diffusion layer, the wavelength of unstable perturbations increases almost linearly from 40 to 93, while if the analogy with

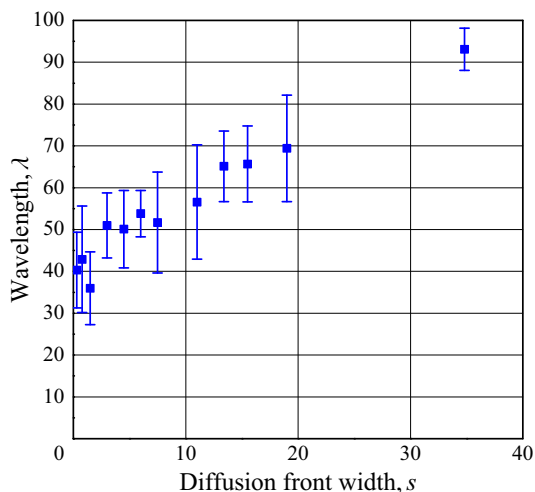


Figure 15. Wavelength vs diffusion front width. Error bars show σ .

Rosensweig's instability were valid, then the wavelength should decrease. Note that, as will be shown below, in the experiment, the distance between the peaks also increases with the thickness of the diffusion front. This fact confirms that the constructed model without surface tension adequately describes the instability of the diffusion front.

Thus, we can conclude that the analogy with the Rosensweig instability does not explain the formation of peaks at the interface of mixing magnetic and non-magnetic fluids in a magnetic field, which occurs on the basis of the balance of gravitational forces, diffusion fluxes and magnetic field energy.

6. Experimental results and discussion

In experimental studies, a magnetic fluid was used, which is a dispersion of magnetite nanoparticles in kerosene, stabilized with oleic acid. The properties of the magnetic fluid are presented in [table 1](#). The magnetic properties of the fluid were obtained with a Lake Shore Cryotronics 7410 VSM vibrating sample magnetometer, density was measured with a Termex vibrating density meter and viscosity with a Rheotest RN 4.1 rotational viscometer. The diffusion coefficient of nanoparticles was measured using a Photocor Complex dynamic and static light scattering spectrometer.

The magnetic fluid was placed in a thin flat cell made of two rectangular transparent Plexiglas plates. The cell width was 25 mm, the height was 15 mm and the distance between the plates was 0.19 mm. The cell was installed vertically. The introduction of liquids into the cell was carried out using a syringe, through which a slow inflow of liquid was carried out simultaneously from the upper left and right edges of the cell. The liquid supplied through the syringe was drawn into the cell due to the capillarity effect. First, a magnetic fluid was introduced, and then kerosene, which was spread over the magnetic fluid during retraction into the cell. As a result of the described procedure, the boundary of liquids with an initially non-zero thickness of the diffuse transition layer between them was obtained. With each new filling of the cell, the thickness of the diffuse layer was reproduced well and amounted to $\approx 100 \mu\text{m}$. To obtain higher values of the diffuse layer thickness, a subcritical magnetic field was applied perpendicular to the liquids' interface. The duration of the field exposure was varied to obtain different values of the diffuse

Instability of diffusion front of miscible magnetic fluid

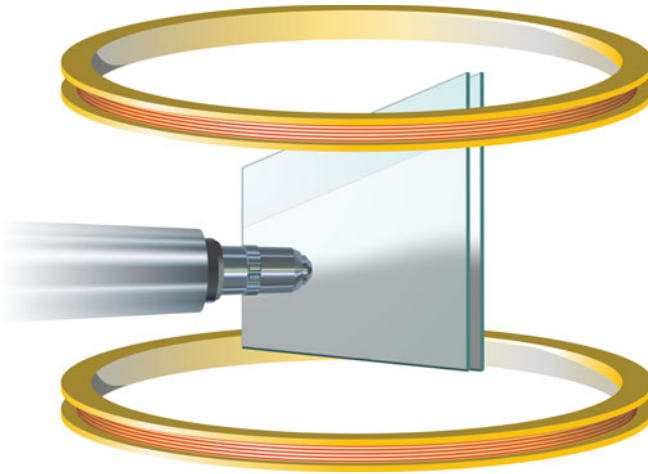


Figure 16. Sketch of the experimental set-up.

layer thickness. It should be noted that this procedure for varying the thickness of the diffuse layer has a low reproducibility of the results obtained. Therefore, in the experiments, the actual thickness of the diffuse layer at the moment was determined each time and then the corresponding experiment was performed. The thickness of the kerosene layer in the experiments was always much greater than the thickness of the magnetic fluid layer. As a result, a horizontal quasi-two-dimensional interface of a magnetic fluid and a pure dispersion medium was formed. The cell was placed in a uniform magnetic field directed vertically and generated by Helmholtz coils. Observation of the dynamics of the boundary between magnetic and non-magnetic fluids was carried out using an optical microscope. The installation sketch is shown in [figure 16](#).

When the magnetic field was turned on, the settling time to the specified value did not exceed 0.01 s. After switching on the magnetic field, the boundary of the magnetic and non-magnetic fluids was deformed, then peaks appeared on it, directed from the magnetic fluid towards the non-magnetic medium. The peaks formed at the initial moment could then divide, splitting into smaller structures resembling a system of needles in shape. The formation of the peaks was accompanied by intense mixing of the liquids, as a result of which these peaks ultimately dissolve, forming a horizontally uniform transition layer between the magnetic and non-magnetic fluids. The parameters of the developing instability (wavelength, peak growth rate, etc.) substantially depend on the magnitude of the magnetic field, the thickness of the diffuse transition layer between fluids δ and the depth of the magnetic fluid layer. As an example, photographs of the change in the shape of the diffusion front at various parameters of the system are shown in [figure 17](#). The dynamics of the developing instability at various values of the magnetic field is illustrated in the attached movie. The observations were carried out in the central part of the cell, and the occurring instability developed simultaneously over the entire section of the liquid boundary under consideration. In this case, the scales of the occurring structures were significantly less than the cell dimensions, which indicates the possibility of neglecting the edge effects in further analysis.

Quantitative estimation of the thickness of the diffuse transition layer between fluids and the depth of the magnetic fluid layer was carried out on the basis of the obtained photographic images. For this, the image was converted to a grey scale format, the area of the image occupied by white pixels was identified with a non-magnetic fluid, the area

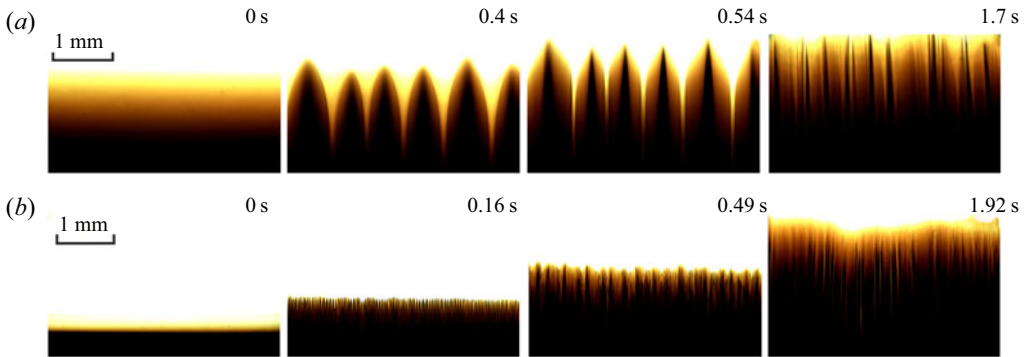


Figure 17. Evolution of the boundary of mixing magnetic and non-magnetic fluids in a normal magnetic field: (a) a wide diffuse layer, $H = 11 \text{ kA m}^{-1}$, $\delta = 1.2 \text{ mm}$; (b) narrow diffuse layer, $H = 5.8 \text{ kA m}^{-1}$, $\delta = 0.1 \text{ mm}$. The results are for the semi-infinite magnetic fluid layer.

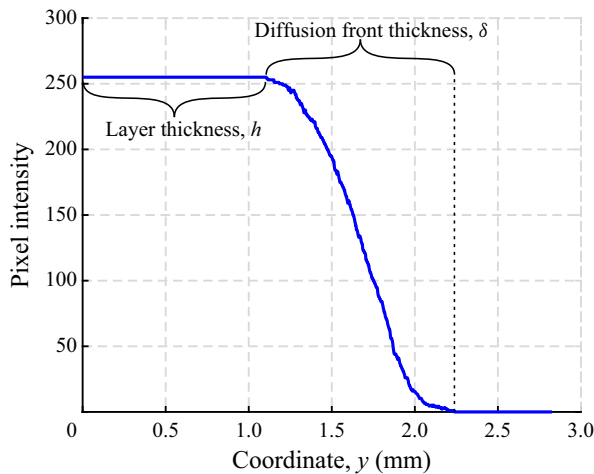


Figure 18. Method for determining the thickness of the diffuse front and the depth of the magnetic fluid layer.

occupied by black pixels was identified with a magnetic fluid of the initial concentration and the area of pixels with intermediate intensity values corresponded to the transition diffuse layer. The depth of the fluid layer was measured from the bottom of the cuvette to the beginning of the diffuse layer (figure 18). Note that the minimum value of the diffuse layer thickness in the experiments was 0.1 mm.

The minimum thickness of the diffusion front achieved in the experiment ($100 \mu \approx 83h_1$) is much greater than the maximum thickness of the diffusion front in the numerical simulation ($20 h_1$). Therefore, it is impossible to quantitatively compare the experimental data with the results of numerical simulation. The main focus was on their qualitative comparison and congruence.

It was found that there is a threshold value of the magnetic field strength at which the development of instability of the interface of mixing magnetic and non-magnetic fluids is possible. As the critical value, such values of the magnetic field strength were chosen at which the deformation of the diffusion front became visually perceptible. It should be noted that, in experiments, the field of a certain value had to be applied abruptly, since a smooth increase in the field led to an increase in the thickness of the

Instability of diffusion front of miscible magnetic fluid

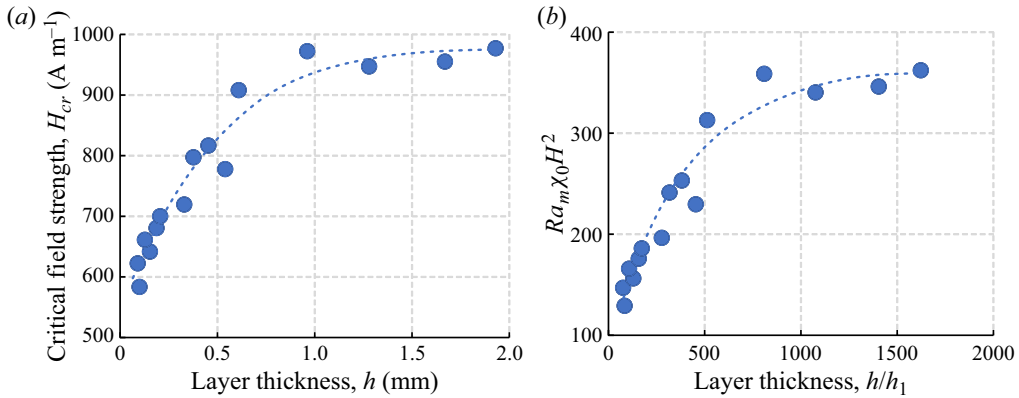


Figure 19. (a) Dimension and (b) dimensionless dependence of the critical value of the magnetic field strength on the depth of the magnetic fluid layer.

diffuse layer and a change in the experimental conditions. Therefore, the critical field was found by sequentially reducing the interval between the value of the field at which the instability does not yet occur and the value of the field at which the interface deformation is distinguishable. The minimum achievable width of such an interval in experiments was 100 A m^{-1} , and the critical field value was selected in the middle of this interval. Measurements were made of the dependence of the critical magnetic field strength on the depth of the magnetic fluid layer and the thickness of the diffuse layer. Note that, at subcritical strengths, there is an intensification of both the mixing of liquids in comparison with diffusion in the absence of a magnetic field and the expansion of the diffusion front, but the interface shape remains visually flat. A similar situation was observed in numerical simulation: at subcritical values of the magnetic field, a system of vortices appeared in the central part of the container, which was not associated with vortices at the edges of the container, but the diffusion front remained flat. This system of vortices facilitates the more rapid expansion of the diffusion front.

Figure 19 shows the dependence of the critical magnetic field strength on the depth of the magnetic fluid layer obtained at minimal diffusion front thickness. This dependence is monotonic. When the depth of the magnetic fluid layer is more than 1 mm, the instability threshold does not depend on the depth. In order to present the data in dimensionless form (figure 19b), the $Ra_m \chi_0 H^2$ criterion was used, since the critical value of the magnetic field (figure 19a) is small and $f(H) = \chi_0 H$.

With an increase in the thickness of the diffuse front δ , the critical magnetic field strength increases (figure 20). In this case, the depth of the magnetic fluid layer was chosen sufficiently large (much larger than the characteristic scale of the arising boundary disturbances), so that the layer in this case can be considered as semi-infinite.

The regularities of the development of instability of the diffusion interface of magnetic and non-magnetic liquids in the supercritical region of values of the magnetic field are studied. The time of development of the instability was measured, which was taken as the time interval from the moment of switching on the magnetic field to the moment when the disturbance of the boundary became visually perceptible. Figure 21 shows the experimental dependences of the development time of instability on the thickness of the diffuse front, obtained at two values of the magnetic field strength. As can be seen from the figure, with an increase in the thickness of the diffuse layer, the development time

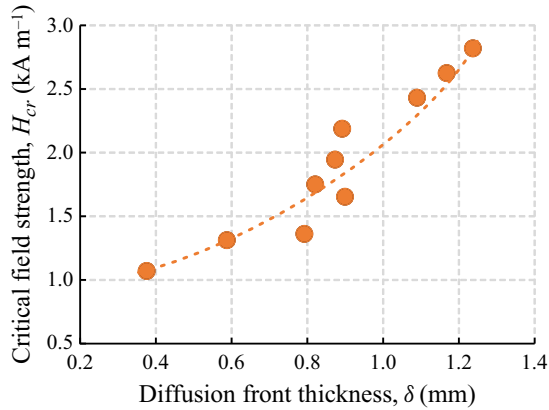


Figure 20. Dependence of the critical value of the magnetic field strength on the thickness of the diffuse front.

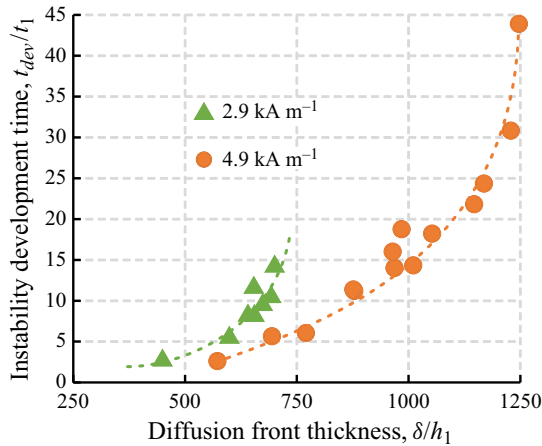


Figure 21. Dimensionless dependence of the development time of instability on the thickness of the diffuse front.

increases monotonically, and decreases with an increase in the field strength. The depth of the magnetic fluid layer in these experiments was quite large.

The instability wavelength was measured, which was determined from the distance between adjacent peaks. In this case, the initial moment of the development of instability before the onset of fission and dissolution of peaks was considered. The error of the presented experimental data was determined from the results of multiple repetitions of the described experiments and averaging of the obtained values. The resulting relative error ranged from 10 % to 20 %. Figure 22 shows the dependence of the wavelength on the thickness of the diffuse front, obtained at three values of the magnetic field strength. The measurements were carried out at a great depth of the magnetic fluid layer. It can be seen from the figure that the instability wavelength increases with an increase in the thickness of the diffuse front, and also decreases with an increase in the field strength. This result correlates qualitatively with the numerical simulation data presented in figure 15.

Figure 23 shows the experimentally obtained dependence of the instability wavelength on the depth of the magnetic fluid layer. In this case, the thickness of the diffuse front was

Instability of diffusion front of miscible magnetic fluid

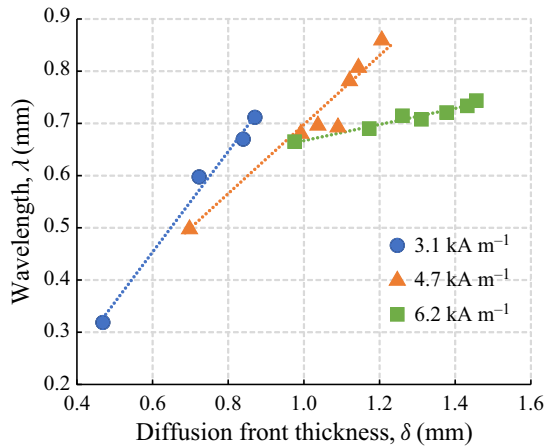


Figure 22. Dependence of the instability wavelength on the thickness of the diffuse front at different values of the magnetic field strength.

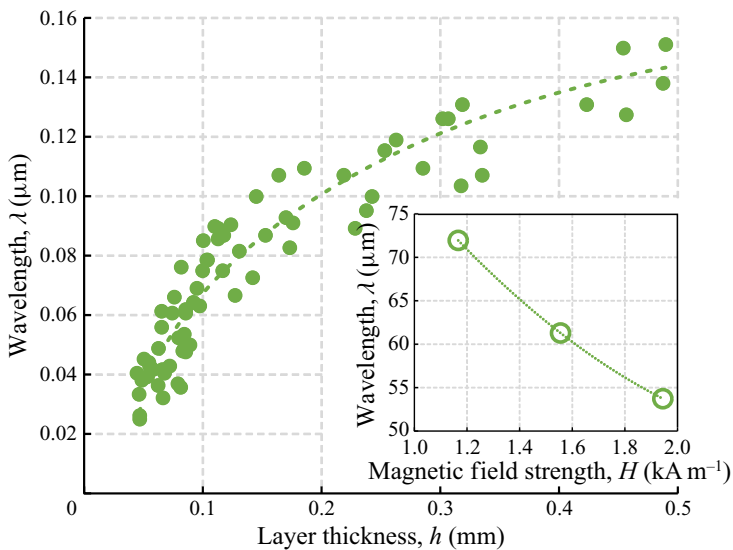


Figure 23. Dependence of the instability wavelength on the depth of the magnetic fluid layer at $H = 1.6 \text{ kA m}^{-1}$. Inset: dependence of the instability wavelength on the magnetic field strength at $h = 0.1 \text{ mm}$ and $\delta = 0.1 \text{ mm}$.

the minimum possible. The wavelength increases with increasing depth of the magnetic fluid layer, which qualitatively agrees with the results of numerical simulation shown in figure 14. The inset in figure 23 shows the dependence of the instability wavelength on the magnetic field strength obtained for the minimum thickness of the diffuse layer and the depth of the magnetic fluid layer equal to 0.1 mm. As for the instability of the free surface of a magnetic fluid bordering on an immiscible medium (Bashtovoi *et al.* 1985; Dikansky *et al.* 2010; Zakinyan *et al.* 2016), this dependence also has a decreasing character. The presented result is in agreement with the simulation data shown in figure 11.

7. Conclusions

The instability of the contact line of miscible magnetic and non-magnetic fluids in a uniform magnetic field normal to the diffusion front is investigated. The study showed that, when the magnetic field strength exceeds a certain threshold value, the plane diffusion front becomes wavy, and then peaks oriented along the magnetic field are formed.

It is shown that, with an increase in the strength of the magnetic field H , switched on instantly, the wavelength of the most unstable disturbances λ decreases.

The effect of the properties of the fluids and magnetic particles is described by the magnetic Rayleigh number Ra_m , the growth of which also leads to a decrease in the distance between the peaks.

The combined effect of the magnetic field and the properties of the liquids is described by the $K_H = f(H)HRa_m$ complex, which takes into account the nonlinear character of the dependence of the magnetization of the fluid on the magnetic field.

It was found that λ decreases with a decrease in the thickness of the magnetic fluid layer and increases with an increase in the thickness of the diffusion front, which differentiates the studied instability from Rosensweig's instability. These results are confirmed both numerically and experimentally.

Supplementary movies. Supplementary movies are available at <https://doi.org/10.1017/jfm.2020.1128>.

Acknowledgements. The authors are thankful to Professor A. Cebers for fruitful discussion on the article.

Funding. A.R.Z. and A.A.Z. acknowledge the support by the Ministry of Science and Higher Education of the Russian Federation in the framework of the governmental ordering to universities for scientific research works (project 751 0795-2020-0030).

Declaration of interests. The authors report no conflict of interest.

Author ORCIDs.

 Mikhail S. Krakov <https://orcid.org/0000-0001-8458-5138>;

 Arthur R. Zakinyan <https://orcid.org/0000-0002-4599-7663>;

 Anastasia A. Zakinyan <https://orcid.org/0000-0003-3170-7351>.

REFERENCES

- BACRI, J.C., SALIN, D. & MASSART, R. 1982 Study of the deformation of ferrofluid droplets in a magnetic field. *J. Phys. Lett.* **43**, 179–184.
- BASHTOVOI, V.G. 1978 Instability of a stationary thin layer of a magnetizable liquid. *J. Appl. Mech. Tech. Phys.* **19**, 65–69.
- BASHTOVOI, V.G., KRAKOV, M.S. & REKS, A.G. 1985 Instability of a flat layer of magnetic liquid for supercritical magnetic fields. *Magneto hydrodynamics* **21** (1), 19–24.
- BERKOVSKY, B.M., MEDVEDEV, V.F. & KRAKOV, M.S. 1993 *Magnetic Fluids: Engineering Applications*. Oxford University Press.
- BRATSUN, D., KOSTAREV, K., MIZEV, A. & MOSHEVA, E. 2015 Concentration-dependent diffusion instability in reactive miscible fluids. *Phys. Rev. E* **92**, 011003(R).
- CAI, G., XUE, L., ZHANG, H. & LIN, J. 2017 A review on micromixers. *Micromachines* **8**, 274–300.
- CAO, Q., HAN, X. & LI, L. 2012 Numerical analysis of magnetic nanoparticle transport in microfluidic systems under the influence of permanent magnets. *J. Phys. D: Appl. Phys.* **45**, 465001.
- CAO, Q., HAN, X. & LI, L. 2015 An active microfluidic mixer utilizing a hybrid gradient magnetic field. *Intl J. Appl. Electromag. Mech.* **47**, 583–592.
- CEBERS, A. 1997 Stability of diffusion fronts of magnetic particles in porous media (Hele-Shaw cell) under the action of external magnetic field. *Magneto hydrodynamics* **33**, 67–74.
- CEBERS, A. & IGONIN, M. 2002 Convective instability of magnetic colloid and forced Rayleigh scattering experiment. *Magneto hydrodynamics* **38**, 265–270.
- COWLEY, M.D. & ROSENSWEIG, R.E. 1967 The interfacial stability of a ferromagnetic fluid. *J. Fluid Mech.* **30**, 671–688.

Instability of diffusion front of miscible magnetic fluid

- DIKANSKY, Y.I., ZAKINYAN, A.R. & MKRTCHYAN, L.S. 2010 Instability of a thin layer of a magnetic fluid in a perpendicular magnetic field. *Tech. Phys.* **55**, 1270–1274.
- ECKERT, K., ACKER, M. & SHI, Y. 2004 Chemical pattern formation driven by a neutralization reaction. I. Mechanism and basic features. *Phys. Fluids* **16**, 385–399.
- ERGLIS, K., TATULCENKOV, A., KITENBERGS, G., PETRICHENKO, O., ERGIN, F.G., WATZ, B.B. & CEBERS, A. 2013 Magnetic field driven micro-convection in the Hele-Shaw cell. *J. Fluid Mech.* **714**, 612–633.
- HURLE, D.T.J. & JAKEMAN, E. 1971 Soret-driven thermosolutal convection. *J. Fluid Mech.* **47** (4), 667–687.
- ISLAM, A., SHARIF, M.A.R. & CARLSON, E.C. 2013 Density driven (including geothermal effect) natural convection of carbon dioxide in brine saturated porous media in the context of geological sequestration. In *2013 Proceedings of the Thirty-Eighth Workshop on Geothermal Reservoir Engineering Stanford University, Stanford, California*, February 11–13, SGP-TR-198. Available at: <https://pangea.stanford.edu/ERE/pdf/IGASstandard/SGW/2013/Islam.pdf>
- IVANOV, A.S. 2019 Experimental verification of anomalous surface tension temperature dependence at the interface between coexisting liquid-gas phases in magnetic and Stockmayer fluids. *Phys. Fluids* **31**, 052001.
- KITENBERGS, G., TATULCENKOV, A., ERGLIS, K., PETRICHENKO, O., PERZYNSKI, R. & CEBERS, A. 2015 Magnetic field driven micro-convection in the Hele-Shaw cell: the Brinkman model and its comparison with experiment. *J. Fluid Mech.* **774**, 170–191.
- KITENBERGS, G., TATULCENKOV, A., PUKINA, L. & CEBERS, A. 2018 Gravity effects on mixing with magnetic micro-convection in microfluidics. *Eur. Phys. J. E* **41**, 138–148.
- KORTEWEG, D.J. 1901 Sur la forme que prennent les équations du mouvements des fluides si l'on tient compte des forces capillaires causées par des variations de densité considérables mais connues et sur la théorie de la capillarité dans l'hypothèse d'une variation continue de la densité. *Arch. Néerl. Sci. Exact. Nat.* **6**, 1–24.
- PATANKAR, S. 1980 *Numerical Heat Transfer and Fluid Flow*. Hemisphere Series on Computational Methods in Mechanics and Thermal Science. Taylor & Francis.
- SCHECHTER, R.S., PRIGOGINE, I. & HAMM, J.R. 1972 Thermal diffusion and convective stability. *Phys. Fluids* **15** (3), 379–386.
- TURNER, J.S. 1985 Multicomponent convection. *Annu. Rev. Fluid Mech.* **17**, 11–44.
- VAND, V. 1948 Viscosity of solutions and suspensions. I. Theory. *J. Phys. Colloid Chem.* **52**, 277–299.
- VISLOVICH, A.N. 1990 Phenomenological equation of static magnetization of magnetic fluids. *Magneto hydrodynamics* **26**, 178–183.
- ZAKINYAN, A., MKRTCHYAN, L. & DIKANSKY, Y. 2016 Experimental investigation of surface instability of a thin layer of a magnetic fluid. *Eur. J. Mech. (B/Fluids)* **56**, 172–177.
- ZELDOVICH, Y.B. 1949 About surface tension of a boundary between two miscible fluids. *Zhurnal Fizicheskoi Khimii (J. Phys. Chem.)* **23**, 931–935 (in Russian).
- ZHU, G.P. & NGUYEN, N.T. 2012 Rapid magnetofluidic mixing in a uniform magnetic field. *Lab on a Chip* **12**, 4772–4780.